PHYSICAL REVIEW D **89,** 073015 (2014)

# Neutrino-nucleus interaction models and their impact on oscillation analyses

P. Coloma,* P. Huber, C.-M. Jen, and C. Mariani

*Center for Neutrino Physics, Virginia Polytechnic Institute and State University, Blacksburg, Virginia 24061, USA*

(Received 6 December 2013; revised manuscript received 7 March 2014; published 17 April 2014)

In neutrino oscillation experiments, neutrino interactions at the detector are simulated using event generators which attempt to reflect our understanding of nuclear physics. We study the impact of different neutrino interactions and nuclear models on the determination of neutrino oscillation parameters. We use two independent neutrino event generators, Generates Events for Neutrino Interaction Experiments (GENIE) 2.8.0 and Giessen Boltzmann-Uehling-Uhlenbeck (GiBUU) 2.6, and apply them to a setup with a conventional neutrino beam aiming at a water Čerenkov detector, for which only the charged-current quasielastic–like sample is selected. Subsequently, we perform a fit to the oscillation parameters in the $\nu_\mu$ disappearance channel.

DOI: 10.1103/PhysRevD.89.073015 PACS numbers: 14.60.Pq, 14.60.Lm

## I. INTRODUCTION

Neutrino physics in the past two decades has seen an astounding transformation from a collection of anomalies to precision science, which most recently resulted in the measurement of $\theta_{13}$ at accelerator [1] and reactor [2–4] experiments. The next goals in neutrino oscillation physics are the determination of the mass hierarchy (i.e., the ordering of the neutrino mass eigenstates) and of the leptonic charge parity ($CP$) phase, which will require control of systematic errors at an unprecedented level of accuracy in neutrino physics. In particular, the measurement of the $CP$ phase will put very stringent demands on the determination of neutrino versus antineutrino interactions in the GeV region; see e.g. Refs. [5–10]. It is widely recognized that our current understanding of nuclear effects in neutrino-nucleus interactions is insufficient to guarantee the required control of systematical errors. A number of studies have been performed focusing on nuclear effects in this context; see for instance Refs. [11–15]. Given the complexity of the full problem with respect to neutrino and antineutrino cross sections, we investigate here the simpler case of $\nu_\mu$ disappearance. In particular, we extend the results of Ref. [16] and perform a comparison of *different* nuclear models and their impact on oscillation parameters. It is a common approach to estimate errors arising from theories using several available theoretical calculations and to take the spread in their results as a measure of the associated uncertainty; we follow the same logic and, specifically, will compare the results obtained using Generates Events for Neutrino Interaction Experiments 2.8.0 (GENIE) [17] and Giessen Boltzmann-Uehling-Uhlenbeck 2.6 (GiBUU) [18,19]. Clearly, this type of intercomparison can be extended to a larger number of event generators as well. Our choice is largely guided by the fact that GENIE is widely used, and GiBUU represents a unique and complementary theoretical approach based on transport theory. Moreover, both codes are open sources which seem a necessary condition for meaningful comparisons. We evaluate the impact of several aspects of nuclear models and their differing implementation with respect to the ability to measure the so-called atmospheric parameters, $\Delta m^2_{31}$ and $\theta_{23}$, in an experimental setup which is similar to T2K. Our main result is that effects from changing the target nucleus from carbon to oxygen induces a bias in $\Delta m^2_{31}$ of about $1\sigma$. Fitting data obtained with one generator and the other results in dramatic shifts due to different modeling and implementation of final state interactions and nuclear models. Also, the absence of multinucleon correlations in the fit can induce a bias between $1\sigma$ and $3\sigma$ on the results for both of the oscillation parameters. As previously found in Ref. [16], a near detector does not resolve these issues.

The paper is organized as follows. In Sec. II, we outline the principle of energy reconstruction for charged-current (CC) quasielastic-like (QE-like) events, and in Sec. III we perform a detailed comparison of the various physics models implemented in both generators for a number of relevant interaction models. This is followed by a detailed description of the simulations in Sec. IV which leads to our results in Sec. V. Finally, in Sec. VI we present our conclusions.

## II. THE QE-LIKE EVENT SAMPLE

In a water Čerenkov detector, the event sample is restricted to CC QE-like events, a definition which was first introduced in Refs. [20–22]. These are selected by requiring that there be only one charged particle above Čerenkov threshold in the final state, the so-called "single ring" events. For a charged-current quasielastic (QE) event considering the neutron at rest, the neutrino energy can be reconstructed from the kinematic variables of the charged lepton $\ell$ in the final state as

*pcoloma@vt.edu

 

$$E_\nu^{QE} = \frac{2(M_n - E_b)E_\ell - (E_b^2 - 2M_n E_b + \Delta M^2)}{2(M_n - E_b - E_\ell + p_\ell \cos\theta_\ell)}, \quad (1)$$

where $M_n$ is the free neutron rest mass, $\Delta M^2 = M_n^2 - M_p^2 + m_\ell^2$, and $E_b$ is the binding energy. Both GENIE and GiBUU use $E_b = 30$ MeV, a value which is obtained from electron scattering data [23,24]. Equation (1) is exact only for the QE interaction with a neutron at rest. However, for any neutrino experiment observing QE-like events, the final sample will also contain events that are not QE. For example, in a single pion neutrino interaction, i.e., an event with a charged lepton and a pion in the final state, the pion can be absorbed by the nucleus during final state interactions (FSI). Such an event will therefore be classified as QE like. In this case, if Eq. (1) is used to reconstruct the neutrino energy, it will unavoidably lead to a value of the reconstructed neutrino energy *lower* than the true incident value for the reason that part of the neutrino energy is carried away by the pion and eventually absorbed by the nucleus. The actual value of the reconstructed neutrino energy will depend on the energy of unobserved particles in the final state [25]. Therefore, while the reconstructed energy will mostly coincide with the true energy of the incident neutrino for a true QE event, there exists a certain probability to have a non-QE event end up being reconstructed with a significantly different neutrino energy. This defines a migration matrix between true and reconstructed neutrino energies, $N(E^{\text{rec}}, E^{\text{true}})$, where each element represents the probability that an event for each given true neutrino energy $E^{\text{true}}$ ends up being reconstructed with a different energy, $E^{\text{rec}}$. The final QE-like event sample will comprise QE as well as non-QE events, where pions are not present in the final state:

$$\begin{aligned} N_i^{QE\text{-like}} &= \sum_j M_{ij}^{QE} N_j^{QE} + \sum_{\text{non-}QE} \sum_j M_{ij}^{\text{non-}QE} N_j^{\text{non-}QE} \\ &\propto \sum_j M_{ij}^{QE} \phi_\alpha(E_j) P_{\alpha\beta}(E_j) \sigma_\beta^{QE}(E_j) \\ &\quad + \sum_{\text{non-}QE} \sum_j M_{ij}^{\text{non-}QE} \phi_\alpha(E_j) P_{\alpha\beta}(E_j) \sigma_{\beta,0\pi}^{\text{non-}QE}(E_j), \end{aligned} \quad (2)$$

where $E_j$ is the true neutrino energy, $P_{\alpha\beta}$ stands for the oscillation probability of $\nu_\alpha \to \nu_\beta$, $\phi(E_j)$ is the initial flavor neutrino flux, and the matrices $M_{ij} \equiv N(E_i^{\text{rec}}, E_j^{\text{true}})$ account for the probability that an event with a true neutrino energy in the bin $j$ ends up being reconstructed in the energy bin $i$. $\sigma_{0\pi}^{\text{non-}QE}$ stands for the cross section for a given non-QE process in which there are no pions in the final state. In this work, we will study a muon neutrino disappearance experiment, so $\alpha = \beta = \mu$.

Finally, it should be kept in mind the classification of event types in neutrino experiments is not well defined, since the incident neutrino energy is not known. In this work, we focus on the migration of non-QE events into the QE-like sample. However, it should be kept in mind that there is a second source of misidentifying events which take place in the opposite direction; for instance, an initially purely QE interaction, where the outgoing proton reinteracts inside the nucleus, producing a Delta resonance ($\Delta$). The $\Delta$ will then decay and produce a pion in the final state. As a result, this event will be classified as non-QE due to the resonance production. In summary, both the QE and resonance interactions are entangled, and sometimes it is hard to distinguish one from the other. Neutrino oscillation experiments rely on different event generators to help them estimate the portion of misidentified QE and resonance production events. However, there are considerable theoretical uncertainties in predicting both event classes. This results in different event generators having different theoretical implementations of the same event types. This is a major source of systematic uncertainty which, like all theory-related errors, is difficult to quantify.

## III. EVENT GENERATORS

In this work, both migration matrices and cross sections in Eq. 2 are computed by the event generator. We have considered two different event generators in this work: GENIE [17] and GiBUU [18,19]. GENIE is used by the major neutrino accelerator experiments in the US, such as MINERvA [26], MINOS [27], MicroBooNE [28], NO$\nu$A [29], and LBNE [30,31], and is also used by the T2K [5] experiment.[1] GiBUU, on the other hand, is based on a semiclassical transport model [19], and therefore constitutes a complimentary and independent theoretical approach.

Figure 1 shows the total cross sections per neutron on $^{16}$O with no pions in the final state for all QE-like interactions using GENIE and GiBUU. In this work, we consider QE, charged-current single pion production (RES) from $\Delta$ resonant decay, charged-current nonresonant pion production (non-RES), and neutrino interactions involving the two-nucleon currents arising from meson exchange processes and nucleon-nucleon correlations (MEC/2p2h). We analyze simulated events with the additional requirement of no pion in the final state. It should be noted that we do not consider the contributions of deep inelastic scattering (DIS) and the production of higher resonances, even though they were included in the analysis performed in Ref. [16]. The reason for this is the following. The cross section for the production of higher resonances with no pion in the final state is found to be very small, see Fig. 1 in Ref. [16], and so is its contribution to the total number of events. In addition, for the particular setup in this simulation work, the neutrino flux decreases very rapidly above 1–1.5 GeV, where the DIS cross section is still negligible.

[1] T2K also uses an independent event generator, neutrino interaction simulation program at Super-K [32].

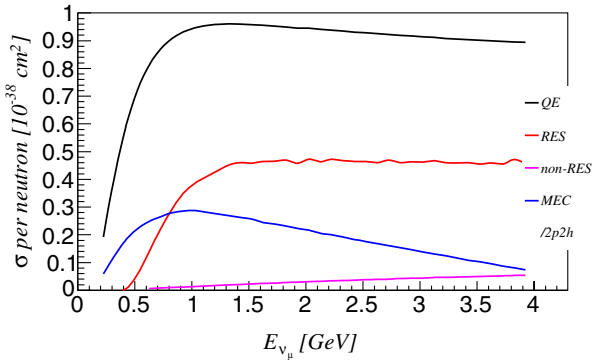


(a)

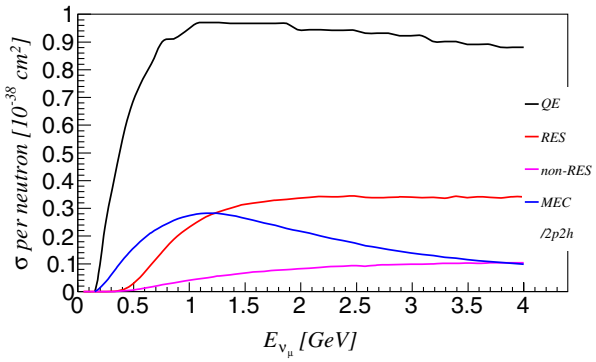


(b)

FIG. 1 (color online). Total cross sections per neutron as a function of the true neutrino energy for different charged-current processes on $^{16}$O after requiring no pion in the final state. Results are shown for GENIE and GiBUU in panels (a) and (b), respectively. Note, RES here only represents the Δ-resonant pion production without including the heavier resonance modes into consideration. Non-RES in panel (a/GENIE) includes the exclusive coherent pion production, while in panel (b/GiBUU) includes only the incoherent part.

Therefore, since there is no sizable contribution from DIS events either, they have been removed from our simulations. It should be kept in mind, though, that the removal of events coming from the higher resonances and DIS may not be the case for neutrino experiments in which the flux peaks at higher energies, such as LBNE [30,31].

The migration matrices are computed as follows. Each neutrino interaction sample consists of 50,000 events, generated in bins of true neutrino energy from 0.2 GeV to 4.8 GeV, for a total of 46 bins. Each matrix is built by counting the number of entries in each bin of the reconstruction energy as defined in Eq. 1 and then dividing it by the total amount of entries. This is done separately for each type of interaction as defined in Fig. 1. For each given value of the initial true energy, a probability distribution in reconstructed energies $\rho^E_{\rm rec}$ can be computed. In fact, $N(E^{\rm rec}, E^{\rm true})$ can be regarded as filling a two-dimensional probability density plane where the y axis indicates the density in reconstructed energies, $\rho^E_{\rm rec}$, and the x axis represents the true energy value. This effectively implements an energy smearing due to nuclear effects. We require the sum of densities for a given true energy to be normalized to the unity, so that the number of events before and after migration remains the same.

Both GENIE and GiBUU event generators differ on the nuclear models used as well as on how the different types of interactions are computed. In the rest of this section, we list some of the main differences between them.

### A. Nuclear model

When generating neutrino-nucleus QE interactions, both GENIE and GiBUU use variants of the relativistic Fermi gas model (RFG) [33] to describe the nuclear structure and the dynamics of neutrino-nucleus interactions under the hypothesis of plane wave impulse approximation (PWIA); see for instance Ref. [34] for a review. In the PWIA, the struck nucleon in every single neutrino-nucleus interaction is treated as a quasifree particle due to the high momentum transfer $Q^2$, while the rest of the nucleus, the so-called spectator system, is left unperturbed. In the RFG, the double differential cross section can be written down as a function of the scattering angle and outgoing lepton's total energy, which is approximated as the lepton's kinematic energy [35]:

$$\frac{d^2\sigma_{\rm IA}}{d\Omega dE_l} = \int d^3p dE P_{RFG}(\mathbf{p}, E)\frac{d^2\sigma_{\rm elem}}{d\Omega dE_l}, \tag{3}$$

with

$$P_{RFG}(\mathbf{p}, E) = \frac{6\pi^2 A}{p_F^3}\theta(\mathrm{p_F} - \mathbf{p})\delta(\Delta E),$$

where $6\pi^2 A/p_F^3$ is a normalization factor, and $p_F$ is the Fermi momentum (221 MeV, or 1.12 fm$^{-1}$), which is the same for all nuclear targets in GENIE and GiBUU. $\Delta E = (E_p - E_b + E)$, where $E_b$ is the average binding energies (i.e., the binding energy of the nucleon). $\sigma_{\rm elem}$ is the elementary cross section used to describe the probability of interactions between the incident neutrino and the nucleon. The integration limits in Eq. 3 are determined by the boundaries of the kinematically allowed region [36].

### B. Quasielastic scattering

The nuclear model used in GENIE to simulate QE interactions is a modified RFG that includes short-range nucleon-nucleon correlations according to the model developed by A. Bodek and J. L. Ritchie [37]. GiBUU also uses the RFG, but, in this case, the RFG is modified by adding corrections from the nucleon's momentum and density dependent mean-field potential, where all nucleons are considered to be bound. The phase-space density function in GiBUU also includes the real part of the self energy for

the knock-out nucleon [38]. Both generators use the same value for the axial mass, $M_A = 1$ GeV/$c^2$.

The vector form factor in GENIE is BBBA05 [39], while in GiBUU it is BBBA07 [40]. The QE cross sections for the two generators are practically the same but with small discrepancies which result from different electromagnetic form factor shapes and separate corrections added to the RFG. The QE event distribution for GENIE and GiBUU on $^{16}$O is shown in Fig. 2.

We have noted some differences in the event distribution as a function of reconstructed neutrino energy between GENIE and GiBUU as shown in Fig. 2. The nuclear model used to describe the QE neutrino interactions is essentially the same between GENIE and GiBUU. For example, we find no differences in the QE cross section as shown in Fig. 1 between GENIE and GiBUU. We do not find any shift between the event distributions as a function of reconstructed neutrino energy if we repeat the same simulation but remove FSI effects for both GENIE and GiBUU. Nevertheless, we find a shift of 10% between the event distribution as a function of reconstructed neutrino energy [defined as in Eq. (1)] between GENIE and GiBUU, as is shown in Fig. 2. This is not surprising due to the fact that GENIE and GiBUU follow a completely different approach to describe FSI. For example in GiBUU, the FSI is modeled by solving the semiclassical Boltzmann-Uehling-Uhlenbeck equation. For more details on GENIE and GiBUU, see for instance Refs. [17,18,41].

The migration matrices for QE events are shown in Fig. 7(a) and Fig. 8(a) in App. B for GENIE and GiBUU, respectively. These matrices include FSI effects.

### C. Meson production via baryon resonances

At the neutrino energies relevant for this work (∼1 GeV), the second dominant neutrino interaction is the single pion production via RES. The RES includes (1) the baryon resonance decay; (2) the charge-exchange of a neutral pion inside the nucleus; and (3) the absorption of multiple pions.

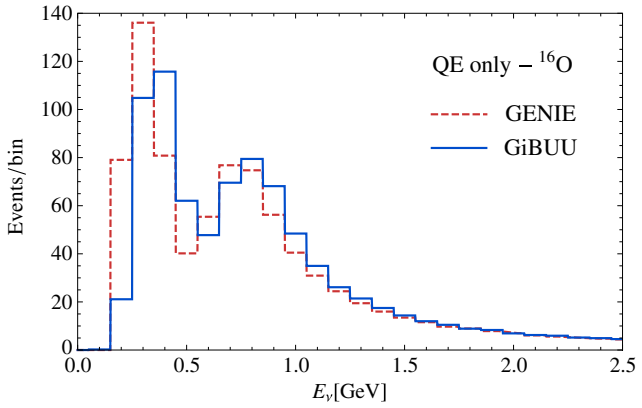


FIG. 2 (color online). Charged-current quasielastic event distributions as a function of the reconstructed neutrino energy for both GENIE (dotted red lines) and GiBUU (solid blue lines). In both cases, oxygen is used as the target nucleus to obtain the cross sections. Both curves include final state interactions, and detector efficiencies have been accounted for.

GiBUU contains 13 kinds of resonance modes. The vector form factors for each resonance mode are obtained from the Mainz Unitary Isobar Model [42,43] analysis of the electron scattering data. The axial form factors for GiBBU are derived from a fit to the data as described in Ref. [44]. In the case of GiBUU, nuclear effects include collisions within nucleons and the nucleon's momentum and density dependent mean-field potential. The FSI is determined by modeling a coupled-channel transport method. This model is tested against electron-, photon-, pion- and proton-scattering data.

GENIE, instead, applies the Rein-Sehgal [45] model with 16 resonance models in the region of transferred energy $W < W_{cut} = 1.7$ GeV. Fermi motion and Pauli blocking are the only nuclear effects included in this case. The FSI is modeled using an intranuclear model as described in detail in Ref. [46]. GENIE RES is validated with electron scattering data from $^{56}$Fe and $^{12}$C targets. The RES event distributions for GENIE and GiBUU using $^{16}$O are shown in Fig. 9(a) in App. B. The corresponding migration matrices are shown in Figs. 7(b) and 8(b) for GENIE and GiBUU, respectively. In Fig. 1, we only show the contribution of Δ-resonant production to the cross section without regarding the heavier resonance modes. As already explained at the beginning of this section, the higher resonance effects become more significant and dominant at higher neutrino beam energies and would therefore have little impact on our results.

### D. Two particles—two holes and meson exchange currents

Aside from QE and RES, at neutrino energies below 1 GeV an additional contribution to the total neutrino cross section comes from processes involving two particle-two hole excitations, as shown in Fig. 1. Several models have been proposed to compute these contributions in neutrino experiments, and the field has been an object of very intense research in the past few years. For an incomplete list of references on this topic, see [22,47–58]. Sources of MEC/2p2h excitation include (1) nucleon-nucleon correlations in the initial state, (2) neutrino coupling to 2p2h and (3) FSI. In processes in which two nucleons are knocked out from the target nucleus, the nucleon's momentum distribution in the spectator system is influenced. Therefore, an excess of QE-inclusive events is produced. Furthermore, it is obvious that if Eq. (1) is applied to obtain the reconstructed neutrino energy, this will most likely differ from the true incident neutrino energy, due to the non-QE nature of the interaction. The effect of 2p-2h has been recently revealed by the theoretical interpretation [22,52] of the results obtained in the MiniBooNE experiment [59].

A detailed description of the implementation of MEC/2p2h in GENIE is available in Ref. [60], and for GiBUU is available in Ref. [55].

The MEC/2p2h event distribution for GENIE and GiBUU on $^{16}$O is shown in Fig. 9(b) of App. B. The associated migration matrices are shown in Figs. 7(c) and 8(c) for GENIE and GiBUU, respectively. These matrices seem to be rather different. To simulate this particular interaction, both GIBUU and GENIE have been tuned based on the measurements on $^{12}$C done by the MiniBooNE experiment and they do not yet include full theoretical model implementations like the ones presented in Refs. [22,47,52,53]. In addition, it should be noted that the MiniBooNE experiment measures the sum of the QE and MEC/2p2h contributions, but the experiment is not capable of discriminating between them. In other words, the tuning of the neutrino interaction generators is performed in such a way that the sum of the QE and the MEC/2p2h contributions to the double differential cross section agrees with the data. Therefore, if a difference exists between GENIE and GiBUU in the QE interactions, then the MEC/2p2h by construction will be different as well. Finally, it is worth mentioning that no difference in the total cross section between GENIE and GiBUU is found for both $^{12}$C and $^{16}$O as a result of the heavy tuning of the model on MiniBooNE $^{12}$C results.

### E. Nonresonant pion production

The non-RES includes the contributions of coherent and noncoherent pion productions. The coherent pion production results in one muon and one single pion in the final state, in which the pion is not produced by a Δ-resonance decay. The residual nucleus system remains in its ground state in the coherent production while in the incoherent pion production this is not the case. GENIE includes only the coherent (exclusive) pion production [61], whereas GiBUU considers only the incoherent pion production process. A full theoretical calculation for this interaction mode can be found in Ref. [62,63].

GENIE uses PCAC [61] with the Rein-Sehgal [64] model to simulate the single pion interaction with the nucleon inside the ground-state target nucleus. The neutrino-nucleon cross section is computed at the initial time ($t = 0$) with the elastic nuclear form factors and an absorption factor to simulate the FSI of the outgoing pion. In contrast, GiBUU takes into account only the incoherent part of the initial-state pion, and does not make any local approximation to the Δ propagator in the medium [61,65]. The non-RES event distribution for GENIE and GiBUU on $^{16}$O is shown in Fig. 9(c) of App. B. The associated migration matrices are shown in Figs. 7(d) and 8(d) for GENIE and GiBUU, respectively.

## IV. SIMULATION DETAILS

In this work we consider a setup very similar to the T2K experiment, simulated following Ref. [66]. The main details of the setup are summarized in Table I. We consider two detectors: a far detector, placed at 295 km from the source, with a fiducial mass of 22.5 kton; and a near detector of 1 kton fiducial mass, placed at 1 km from the decay pipe. The size and location of the near detector have been chosen so as to guarantee that the near detector observes enough events to be able to constrain the systematic errors included in the analysis (for details on the systematic errors and the $\chi^2$ implementation, see App. A). In this work, we assume that the two detectors observe the same flux, and that they are identical in terms of their composition and detection properties. It should be kept in mind, however, that these assumptions would most likely *not* be realized in an actual neutrino beam experiment. This may lead to a *larger* impact of nuclear effects on the extraction of the oscillation parameters than what is found in this work.

TABLE I. Main details for the experimental setup simulated in this work.

| | Baseline | Fiducial mass | Flux peak | Beam power | Running time |
|---|---|---|---|---|---|
| Far | 295 km | 22.5 kt | 0.6 GeV | 750 kW | 5 yrs |
| Near | 1.0 km | 1.0 kt | | | |

The only oscillation channel considered is $\nu_\mu \to \nu_\mu$ disappearance. For this channel, the only relevant background would come from neutral current (NC) interactions. We do include such a background in our analysis, which produces a total of ∼275 events at the far detector. Nevertheless, since our aim is to explore the impact of nuclear effects on the CC signal, we keep the background event rates the same for all the configurations under consideration in this work, and no study is done on the variation of these rates with different nuclear models and/or energy reconstruction effects. Background rates are smeared using a Gaussian with $\sigma(E) = 85$ MeV, following Ref. [66]. For the signal, on the other hand, since the migration matrices due to nuclear effects already introduce a rather coarse energy smearing, we do not consider additional effects due to the finite resolution from the detector. We believe the effect due to this will certainly be minor, considering the large smearing that we observe already for the QE event sample; see Figs. 7(a) and 8(a) in App. B. Finally, energy dependent detection efficiencies are implemented for the signal, following Ref. [66]. These are applied after the events are migrated to reconstructed neutrino energies.

The expected number of events at the far detector for the different contributions to the QE-like event sample are shown in Table II. These are computed using the cross sections produced for the two event generators under consideration, using oxygen as the target nucleus. Figure 3 shows the expected event rates for the QE-like event sample, binned as a function of the neutrino energy.

TABLE II. Total number of events expected at the far detector for the different contributions to the QE-like sample and for the oscillation parameters in Eq. (A1). The expected number of events is shown for the two event generators under consideration. In both cases oxygen is chosen as the target nucleus. Efficiencies are already accounted for. The distribution of events for the different contributions as a function of the reconstructed neutrino energy can be found in App. B.

| | QE | RES | Non-RES | MEC/2p2h | Total |
|---|---|---|---|---|---|
| GiBUU | 870 | 152 | 32 | 214 | 1268 |
| GENIE | 877 | 221 | 11 | 249 | 1358 |

Results are shown for the near and far detectors in the right and left panel, respectively. The gray shaded areas show the event rates for the events before migration to reconstructed energies, while the solid blue (dashed red) lines show the results after migration to reconstructed neutrino energies, when the matrices and cross sections are computed using GiBUU (GENIE), as explained in Sec. III. In all cases, the oscillation parameters have been set to the values in Eq. (A1) in App. A, and detector efficiencies are accounted for. We find that the event distributions using the matrices generated with GiBUU are in agreement with those shown in Fig. 10 of Ref. [13]. Similar results were also shown in Fig. 3 of Ref. [14] for a different nuclear model.[2]

It is also worth mentioning the large contribution to the QE-like sample coming from MEC/2p2h contributions. It has recently been argued [22,52] that this may be the source of the large discrepancy between the value of $M_A$ reported in Ref. [59] and the world average value of $M_A \sim 1.0$ GeV; see for instance Ref. [67]. As it can be seen from Table II [see also Fig. 9(b) in App. B], the expected contribution to the QE-like sample from MEC/2p2h interactions is rather large for the setup considered in this work as well. Table II shows that ∼17% of the final QE-like sample in our simulated setup would come from MEC/2p2h interactions. The difference between the number of events (∼10%) obtained is also noticeable when the cross section is computed using GiBUU or GENIE. This difference is not coming from the size of the cross section, since in both cases the MEC/2p2h cross section is tuned to the MiniBooNE data and the size of the peak is roughly the same; see Fig. 1. The reason for the difference in the number of events is a shift in neutrino energy in the cross section obtained from the two generators when they are compared against each other: while the GENIE cross section reaches its maximum at around 1 GeV, the GiBUU cross section peaks at slightly higher energies, around 1.2 GeV. Since the peak in the neutrino flux considered in this work lies below 1 GeV or so, the number of events from MEC/2p2h interactions when the GENIE cross section is used will be larger. Finally, small differences can also be appreciated in the number of events coming from resonant and nonresonant pion production. The first one comes from a different number of resonances included in the computation; see also Sec. III C. In the second case, a different result is obtained since GiBUU computes incoherent pion production while GENIE computes only the coherent contribution to this process.

[2]It should be noted that, in Fig. 3, the event distribution before migration has been smeared with a Gaussian energy resolution function with a constant width to account for the detector's finite energy resolution. As a result, the lowest two energy bins have slightly more events before migration than after migration. We have checked that for a detector of perfect energy resolution this is not the case and therefore our results are in agreement with those in Refs. [13,14].

## V. RESULTS

In this section, we explore the impact on the extraction of the oscillation parameters in three different scenarios:

(A) when the target nucleus is changed in the fit;
(B) when the nuclear model is changed in the fit;
(C) when MEC/2p2h are completely removed from the fit.

### A. Impact of different target nuclei

It is common practice to "tune" event generators according to a given target nucleus in a certain experiment. However, the event generator may be used later on for an oscillation experiment using a different target. In this section we evaluate the effect on the oscillation analysis if an event generator is tuned according to data obtained for a certain target but the experiment is performed using a different target. Results are shown in Fig. 4. In the left panel, the binned expected event rates are shown as a function of the reconstructed neutrino energy, when oxygen (solid black lines) and carbon (dashed gray lines) are used to compute the cross sections and migration matrices in Eq. (2). In both cases, the GENIE event generator is used to compute the matrices for all contributions. As it can be seen from the figure, there is a slight shift towards lower energies in the event rates for carbon with respect to those obtained for oxygen. We have checked that this shift is already present for the true QE event sample, and that it remains if final state interactions are removed from the simulation. This is automatically translated into a shift for the best fit value of the mass-squared splitting. The effect is shown in the right panel, where the gray shaded areas show the results when the true and the fitted event rates are computed using the same set of migration matrices, while the solid lines show the results when a different target is used to compute the matrices used in the true and the fitted event rates. In our particular example, oxygen is used to generate the matrices and cross sections used to compute the true rates, and these are then fitted using carbon migration matrices and cross sections. As it can be seen from the figure, there is a shift in the best fit for the atmospheric mass splitting from $2.45 \times 10^{-3}$ eV$^2$ to $\sim 2.49 \times 10^{-3}$ eV$^2$.

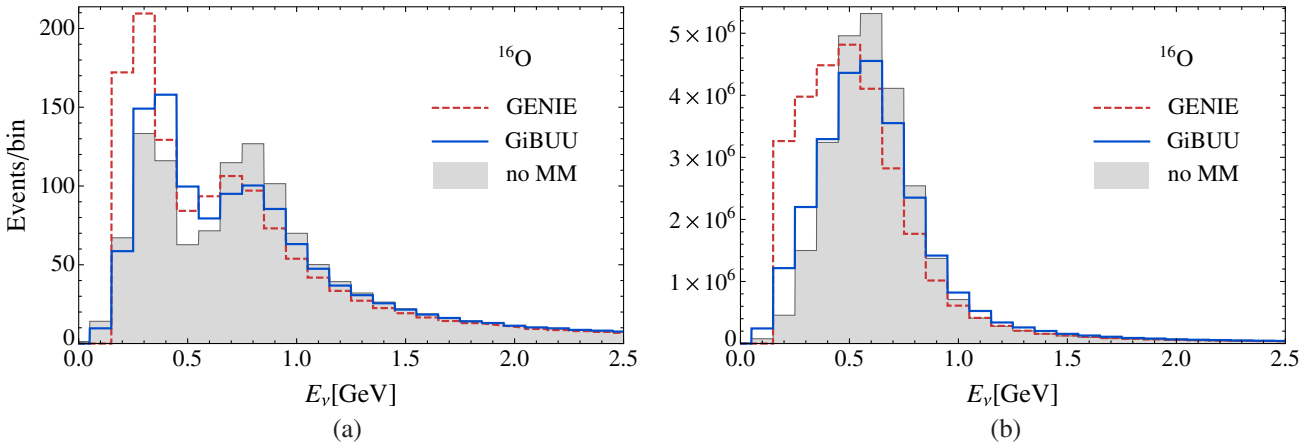


FIG. 3 (color online). Binned QE-like event rates as a function of the reconstructed neutrino energy in GeV, computed using Eq. (2). The solid blue (dashed red) lines show the event rates obtained after migration using the GiBUU (GENIE) event generators. The shaded areas show the expected event rates coming from the QE-like event sample computed using the GiBUU cross section for $^{16}$O, as for the solid blue lines, but without including any migration matrices [i.e., taking $M_{ij}^{QE} = M_{ij}^{\text{non-}QE} = \delta_{ij}$ in Eq. (2)]. For the shaded areas, a Gaussian energy resolution function with a constant standard deviation of 85 MeV is added to account for the finite resolution of the detector. All lines have been obtained for the oscillation parameters in Eq. (A1), and detector efficiencies have already been accounted for. (a) Expected events at the far detector. (b) Expected events at the near detector.

There is also a shift in the best fit for the mixing angle, although in this case the effect is minor. The value of the $\chi^2$ found at the best fit is also shown, together with the number of degrees of freedom in the analysis, $n - p$, where $n$ is the number of energy bins and $p$ is the number of parameters that are being determined from the fit. Finally, it is worth mentioning that we find the size of this effect to be practically negligible if the GiBUU event generator is used to produce the migration matrices and cross sections instead of GENIE.

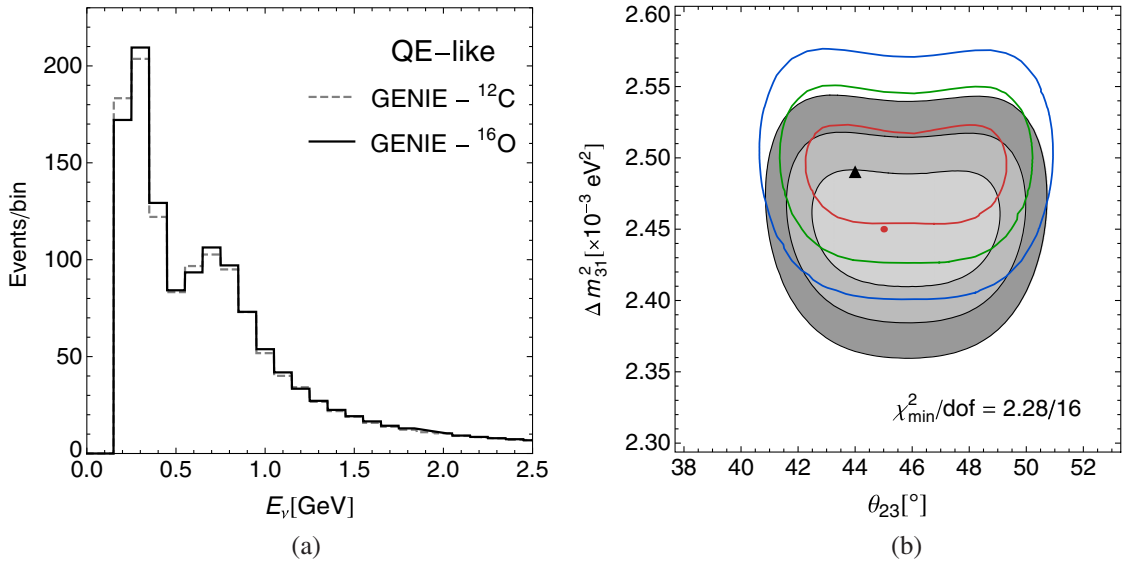


FIG. 4 (color online). Impact on the results if a different target is used to compute the true and fitted rates in the analysis. (a) Event rates per bin obtained using migration matrices computed for oxygen (solid black) or carbon (dashed gray) as the target nucleus. (b) Result of the fit in the in the $\theta_{23} - \Delta m^2_{31}$ plane. The shaded area shows the confidence regions that would be obtained at 1, 2, and 3$\sigma$ if the true and fitted rates are generated using the same set of migration matrices. The colored lines show the resulting regions if the event rates computed using matrices for oxygen (solid lines in the left panel) are fitted with the rates computed using matrices for carbon (dashed lines in the left panel). The GENIE event generator has been used in both cases to generate the migration matrices. The red dot indicates the true input value, while the black triangle shows the location of the best fit point. The value of the $\chi^2$ at the best fit is also shown, together with the number of degrees of freedom.

### B. Impact of different nuclear models

Let us now address the impact of using a different nuclear model. For this purpose, we take the event rates computed using migration matrices produced with one event generator and we try to fit them using the matrices obtained with a different generator. The difference in the event rates when the matrices are computed with different generators is significant, as can be seen from the comparison of the solid blue and dashed red lines in Fig. 3. In fact, we find that the main source of the discrepancy appears in the QE sample already, as discussed in Sec. III. Therefore, a large effect in the fit to the oscillation parameters should be expected in this case. The results are shown in Fig. 5. Again in this case, the shaded regions show the confidence regions when the same set of matrices is used to compute the true and the fitted event rates. For the solid lines, on the other hand, we compute the true event rates using matrices produced with GiBUU, and try to fit them with the event rates computed using the matrices from GENIE. In all cases, oxygen is chosen as the target nucleus. We find that the difference between the two models is so large that the best fit for the atmospheric mass splitting takes place around $2.69 \times 10^{-3}$ eV$^2$, as shown in Fig. 5(a). Such a large value would be in strong tension with the presently allowed region at $3\sigma$ from global fits; see for instance Ref. [68]. The fit would disfavor the true input value for the mass splitting at much more than $3\sigma$ and for the atmospheric mixing angle at roughly $2\sigma$.

In a real experiment, this would most likely be attributed to a systematic error that has not been correctly evaluated, or to a signal of new physics. We focus on the first possibility here. In particular, since we observe that the main difference in the event rates is that the events suffer an energy shift (see Fig. 3 or Fig. 2), we introduce a calibration error as an additional nuisance parameter.[3] In order to do so, the event rates are effectively recomputed as

$$N[E] \to N[(1+a)E],$$

where $a$ is the calibration error. An additional pull term $(a/\sigma_a)^2$ is added to the $\chi^2$ in Eq. (A3), where $\sigma_a$ is the prior uncertainty for this parameter. After a calibration error of around 5% is added, the resulting best fit is in much better agreement with the true input value, as can be seen from Fig. 5(b). Nevertheless, there is still a significant shift in the best fit (black triangle) with respect to the true value (red dot), which brings it from $2.45 \times 10^{-3}$ eV$^2$ to $2.55 \times 10^{-3}$ eV$^2$. The best fit for the mixing angle is also shifted a couple of degrees into the second octant. The value of the $\chi^2$ at the minimum over the number of degrees of freedom is also computed, and found to be $\chi^2_{\rm min}/{\rm dof} \sim 21/16$. We find that the largest contribution to the minimum of the $\chi^2$ comes from the tension in the energy bins below ~0.5 GeV between the two event distributions. This can be understood from the comparison of the event histograms in Fig. 3, where the differences between the solid and dashed lines are observed to be largest in this energy region. In order to accommodate the large differences in these bins, the associated nuisance parameters during the $\chi^2$ minimization tend to take large values. As a consequence, their respective pull-terms will significantly contribute to the final $\chi^2$. Details on the systematics implementation can be found in App. A.

### C. Impact of multinucleon contributions

Recently, a lot of attention has been drawn to the MiniBooNE experiment and the extraction of the value of the axial mass from the QE data. It seems that the ~35% disagreement between the value of the axial mass extracted from the results in[4] Ref. [59] and the one obtained from previous experiments may be explained (at least partially) if multinucleon contributions are included in the analysis; see for instance Refs. [22,53,54]. In this section, we evaluate the impact that neglecting MEC/2p2h contributions may have on the extraction of neutrino oscillation parameters. The results are shown in Fig. 6 when the migration matrices are computed using GiBUU (left panel) and GENIE (right panel). In both cases, oxygen is used as the target nucleus. The shaded areas show the confidence regions at 1, 2, and $3\sigma$ confidence level (C.L.) when all contributions to the QE-like event sample are considered as in Eq. (2), and the same set of migration matrices is used to compute the true and fitted event rates. For the solid lines, on the other hand, the fit is done when the MEC/2p2h contribution is completely removed from the fitted event rates. As expected, the impact on the confidence regions is rather relevant, and induces large deviation for the best fit values of the oscillation parameters, between 1 and $3\sigma$ depending on the event generator that is used to produce the migration matrices.

A final comment is in order here. As it was shown previously in the literature (see for instance Refs. [11–15]) and confirmed here, the energy dependence of the QE-like event sample is very different when MEC/2p2h contributions are included. We have shown in this section that the impact of multinucleon contributions on the extraction of oscillation parameters can be rather large in the disappearance channels. Similar effects are in principle expected in the appearance channels as well. This could have a significant impact on the sensitivity to *CP*

[3]A real experiment, if equipped with calibration methods, will find it very difficult to make such an adjustment. Modern calibration systems have an error of a few % and their results are part of the oscillation analysis.

[4]Recently, the MINERvA collaboration has also observed deviations from the expected result within the RFG model approach [69].

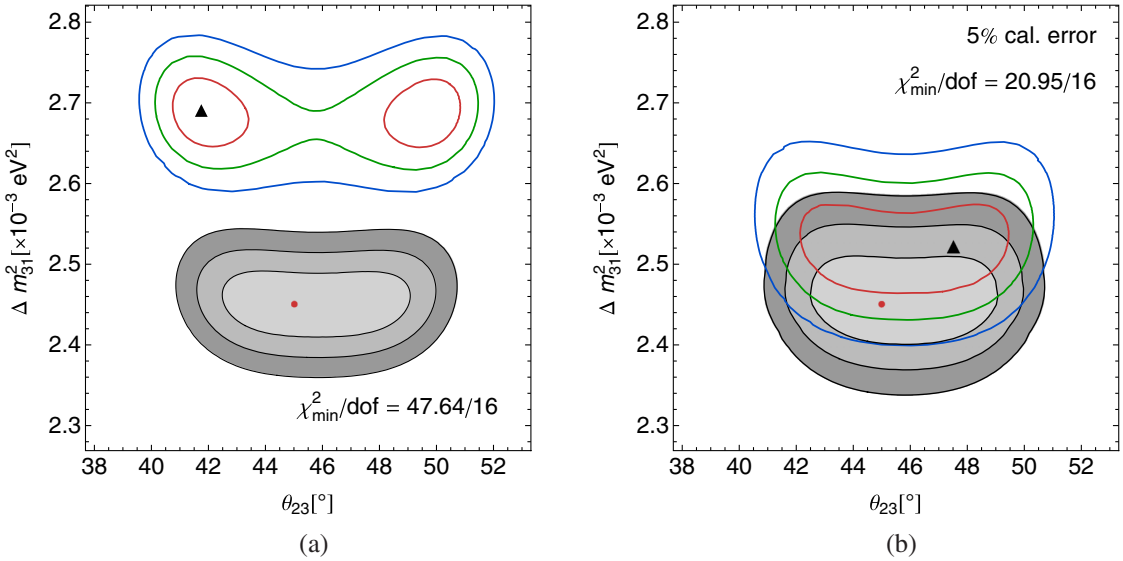


FIG. 5 (color online). Impact on the results if a different generator is used to compute the true and fitted rates in the analysis. The shaded areas show the confidence regions at 1, 2, and 3$\sigma$ that would be obtained in the $\theta_{23} - \Delta m^2_{31}$ plane if the true and fitted rates are generated using the same set of migration matrices (obtained from GiBUU, with oxygen as the target nucleus). The colored lines show the same confidence regions if the true rates are generated using matrices produced with GiBUU, but the fitted rates are computed using matrices produced with GENIE. Both sets of matrices are generated using oxygen as the target nucleus. The red dot indicates the true input value, while the black triangle shows the location of the best fit point. The value of the $\chi^2$ at the best fit is also shown, together with the number of degrees of freedom. In panel (a) no energy scale uncertainty is considered, while in panel (b) an energy scale uncertainty of 5% is assumed; see text for details.

violation at future oscillation experiments (as mentioned, for instance, in Refs. [13–15,70]), since the sensitivity to *CP* violation in neutrino oscillations comes from the analysis of *both* the energy dependence of the signal *and* the comparison between neutrino and antineutrino rates. Both GENIE and GiBUU have tuned their MEC/2p2h interactions to the MiniBooNE data, and their results for MEC/2p2h contributions with oxygen and carbon therefore give exactly the same results. However, *a priori* there is no reason to think that these effects should be the same for different nuclei. As for antineutrinos, there are currently very few measurements available. The MiniBooNE collaboration has recently reported some measurements in the antineutrino channel, where again it seems that MEC/2p2h may play a leading role [71]. This result has also been confirmed by the MINERvA collaboration [72]. Nevertheless, we would like to stress the fact that the current proposals for the next generation of neutrino experiments would use either water (T2HK [73] or ESS$\nu$SB [74], for instance) or liquid argon (LBNE [30,31] and LBNO [75]) detectors, for which there are practically no measurements available at the relevant neutrino energies. Again in this case, theoretical calculations show that in principle one should not expect these effects to be similar for neutrinos and antineutrinos [47,70,76,77], and may be even larger for the latter; see for instance Refs. [70,76].

## VI. CONCLUSIONS

Nuclear effects in neutrino interactions will be one of the leading sources of systematical errors in future neutrino-beam oscillation experiments. Already in the current T2K appearance result they are among the largest contributors to the overall systematic error budget [78]. In this paper we try to estimate the size of the systematic error associated with theoretical models of nuclear effects as embodied by event generators, specifically GENIE and GiBUU. Apart from providing a quantitative estimate, we also developed a methodological framework which lends itself to be extended to a larger class of event generators and in principle also to *CP* violation studies.

Given that LBNE has chosen argon as the detector material, one question is whether changing the nuclear target will have a profound impact on the ability to extract oscillation physics. To get a first glimpse of an answer, we study the $\nu_\mu$ disappearance channel and determine the bias resulting from simulating data with oxygen as a target and fitting those data with a carbon interaction model. The results of this experiment are shown in Fig. 4(b) and the quantitative findings are summarized in Table III, which correspond to a 1$\sigma$ bias in $\Delta m^2_{31}$. These results are only an indication, but it is noteworthy that most nuclear models have been tuned on carbon data and, thus, the generators can be expected to

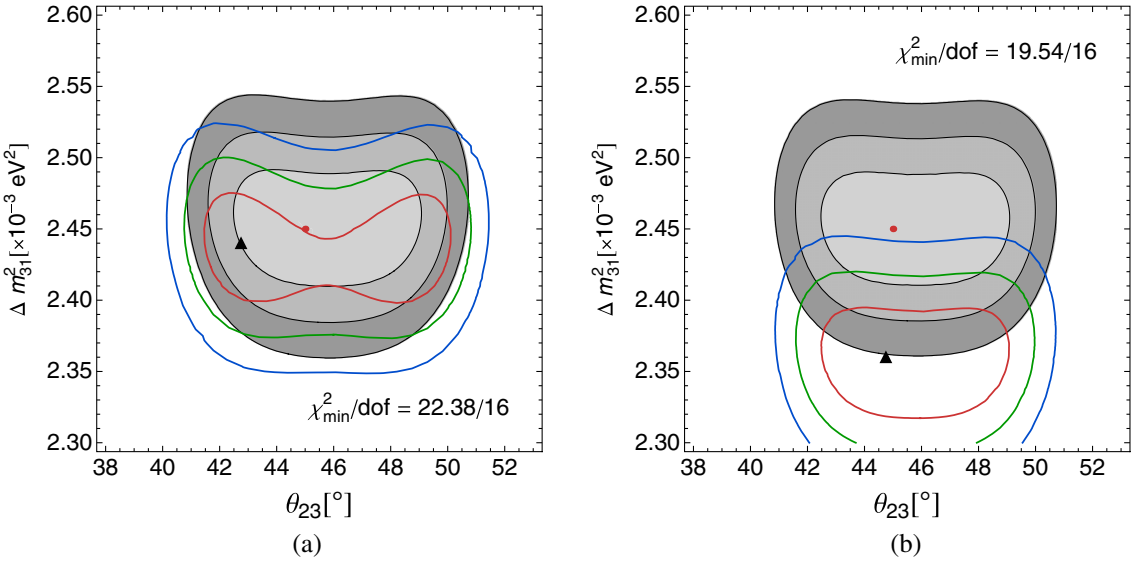


FIG. 6 (color online). Impact on the results if MEC/2p2h interactions are removed from the fit. The shaded areas include all contributions to QE-like events both in the true and fitted rates. The colored lines show the confidence regions at 1, 2, and $3\sigma$ that would be obtained if the true rates are generated including MEC/2p2h interactions, but they are removed from the fitted rates. The results are shown for the GiBUU (a) and for the GENIE (b) event generators. In each case, the red dot indicates the true input value, while the black triangle shows the location of the best fit point. The value of the $\chi^2$ at the best fit is also explicitly shown, together with the number of degrees of freedom. No energy calibration uncertainty has been assumed in this case for any of the panels.

be most accurate for nuclei around carbon. Nevertheless, it is somewhat surprising that a small step in atomic mass from $A = 12$ to $A = 16$ leads already to a sizable bias. What would happen if one tried to extrapolate to argon with $A = 40$ remains pure speculation.

Interestingly, we find even for carbon very large differences in the shape of the QE event rate spectrum between GENIE and GiBUU which we trace back to differences in the implementation of final state interactions; see Sec. III. These differences are large enough to introduce a bias in the mass splitting of many standard deviations. The resulting minimum of the $\chi^2$ would also be very large, as shown in Fig. 5(a). Introducing an uncertainty on the energy scale of 5% reduces the resulting tension and also brings the $\chi^2$ back to acceptable levels, but still leaves a $1\sigma$ bias in both the mass splitting and mixing angle; see Fig. 5(b). Besides, it is also not clear whether an oscillation experiment would have any freedom left to include such a large calibration error in the fit.

Finally, the recent MiniBooNE results seem to imply that multinucleon effects play an important role for neutrino energies $E_\nu \sim \mathcal{O}(\mathrm{GeV})$. There is a large variety of models in the literature trying to describe these effects. Therefore, we test the effect of removing the multinucleon correlation in the fit of data which has been generated including those. This is again a case where the two generators produce different effects—in GiBUU the mixing angle is most affected, whereas in GENIE it is the mass splitting seeing the bulk of the effect, which is obvious from Fig. 6.

TABLE III. Summary of the main impact on the oscillation parameters for the different scenarios studied in this work. The true values for the disappearance oscillation parameters are $\theta_{23} = 45^\circ$ and $\Delta m^2_{31} = 2.45 \times 10^{-3}\ \mathrm{eV}^2$. The number of degrees of freedom in the fit is $n - p = 16$, where $n$ is the number of energy bins and $p$ is the number of oscillation parameters that are being estimated from the fit. Here, $\sigma_a$ represents the prior uncertainty assumed for an energy calibration error, whose implementation is described in Sec. V B.

| True | Fitted | $\theta_{23,\mathrm{min}}$ | $\Delta m^2_{31,\mathrm{min}}[\mathrm{eV}^2]$ | $\chi^2_{\mathrm{min}}$ | $\sigma_a$ | Fig. no. |
|---|---|---|---|---|---|---|
| GENIE ($^{16}$O) | GENIE ($^{12}$C) | 44° | $2.49 \times 10^{-3}$ | 2.28 | – | [4] |
| GiBUU ($^{16}$O) | GENIE ($^{16}$O) | 41.75° | $2.69 \times 10^{-3}$ | 47.64 | – | 5(a) |
| | | 47° | $2.55 \times 10^{-3}$ | 20.95 | 5% | 5(b) |
| GiBUU ($^{16}$O) | GiBUU ($^{16}$O) w/o MEC | 42.5° | $2.44 \times 10^{-3}$ | 22.38 | – | 6(a) |
| GENIE ($^{16}$O) | GENIE ($^{16}$O) w/o MEC | 44.5° | $2.36 \times 10^{-3}$ | 19.54 | – | 6(b) |

In summary, we find that changing nuclear targets, the used event generator or the implementation of multi-nucleon effects, each leaves a bias comparable to the statistical errors in the determination of the mixing parameters, as illustrated in Table III. Any experiment aiming at high precision measurements of oscillation parameters like the leptonic $CP$ phase will have to develop a strategy to deal with these uncertainties in a transparent fashion. One important step in this direction would be to make the event generators accessible to the community. We have only considered light targets like carbon and oxygen and it is unclear how to extrapolate to heavier targets like argon without additional data. The methods presented here are well suited to be extended to experiments aiming to determine the $CP$ phase and the neutrino mass hierarchy.

## ACKNOWLEDGMENTS

The authors thank S. Dytman, U. Mosel, and O. Lalakulich for their support, which lead to successful simulation results. We would also thank D. Meloni, J. Nieves, N. Rocco, and M. Vicente Vacas for useful discussions, and O. Benhar for the precious discussions and for careful reading of this manuscript. This work has been supported by the U.S. Department of Energy under Award No. DE-SC0003915.

## APPENDIX A: $\chi^2$ IMPLEMENTATION

In this appendix we briefly describe the details of the implementation of the $\chi^2$ and the inclusion of systematic uncertainties. All fits to the oscillation parameters presented in Sec. V are performed using GLoBES [79,80]. Unless otherwise stated, the true values of the oscillation parameters are set to the following:

$$\theta_{12} = 33.2^\circ \quad \Delta m^2_{21} = 7.64 \times 10^{-5}\ \text{eV}^2 \quad \theta_{13} = 9^\circ$$
$$\Delta m^2_{31} = 2.45 \times 10^{-3}\ \text{eV}^2 \quad \theta_{23} = 45^\circ \quad \delta = 0^\circ. \quad \text{(A1)}$$

A $\chi^2$ analysis is done to extract the best fit values for the oscillation parameters as well as the allowed confidence regions at 1, 2, and $3\sigma$ C.L. For each energy bin $i$ and detector $D$, a contribution to the $\chi^2$ is computed as

$$\chi^2_{i,D} = 2\left(T_{i,D}(\theta,\xi) - O_{i,D} + O_{i,D}\ln\frac{O_{i,D}}{T_{i,D}(\theta,\xi))}\right), \quad \text{(A2)}$$

with

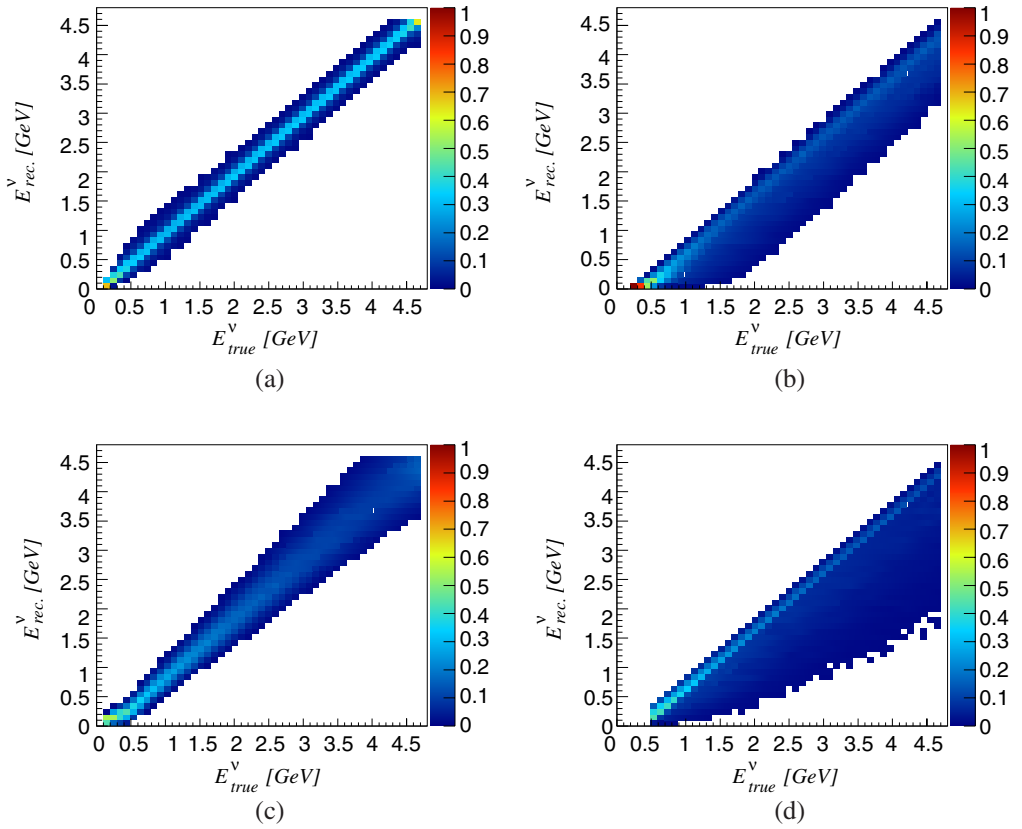


FIG. 7 (color online). Two-dimensional migration matrices ($M_{ij}$), for QE (a), RES (b), MEC/2p2h (c), and non-RES(d) for GENIE, using $^{16}$O as the target nucleus.

$$T_{i,D}(\theta,\xi) = (1 + \xi_n + \xi_{\phi,i}) N_{i,D}(\theta).$$

Here, $O_{i,D}$ ($T_{i,D}$) refer to the true (fitted) event rates observed at a detector $D$ in an energy bin $i$, $\theta$ indicates the dependence on the test values for the oscillation parameters, and $\xi_{\phi,i}$ and $\xi_n$ stand for the nuisance parameters associated to flux and normalization uncertainties, respectively. It should be noted that $O_{i,D}$ depends only on the true values assumed for the oscillation parameters, while $T_{i,D}$ depends on the pair of values we are testing as well as on the nuisance parameters. In addition, the nuisance parameter associated to the normalization error is bin-to-bin correlated, while the one associated to the flux uncertainty is bin-to-bin uncorrelated. These will help to accommodate the normalization and shape differences in the event rates due to different nuclear models. The final $\chi^2$ reads

$$\chi^2 = \min_{\xi}\left\{\sum_{D,i}\chi^2_{i,D}(\theta;\xi) + \left(\frac{\xi_{\phi,i}}{\sigma_\phi}\right)^2 + \left(\frac{\xi_n}{\sigma_n}\right)^2\right\}, \quad \text{(A3)}$$

where the two last terms are the pull-terms associated to the nuisance parameters $\xi$, and $\sigma_\xi$ is the prior uncertainty assumed for each systematic error (which has been set to 20% in all cases). All oscillation parameters are kept fixed during the fit. Since the analysis is done for the disappearance $\nu_\mu \to \nu_\mu$ channel only, we believe that marginalization will not have a relevant impact on our results. Finally, the sum in Eq. (A3) is done over 100 MeV bins between 0.2 and 2.0 GeV. Nevertheless, the migration matrices and cross sections are computed up to ~5 GeV in true neutrino energy in order to get the full contribution from the high-energy tail of the flux.

## APPENDIX B: MIGRATION MATRICES AND EVENT DISTRIBUTIONS

In this appendix we show the complete set of migration matrices used in the oscillation analysis for GENIE (Fig. 7) and GiBUU (Fig. 8) using oxygen as the target nucleus. The number of events as a function of reconstructed neutrino energy for the various neutrino interaction modes, as described in Sec. III, is also shown in Fig. 9 for oxygen. The results for carbon are similar and therefore will not be shown here.

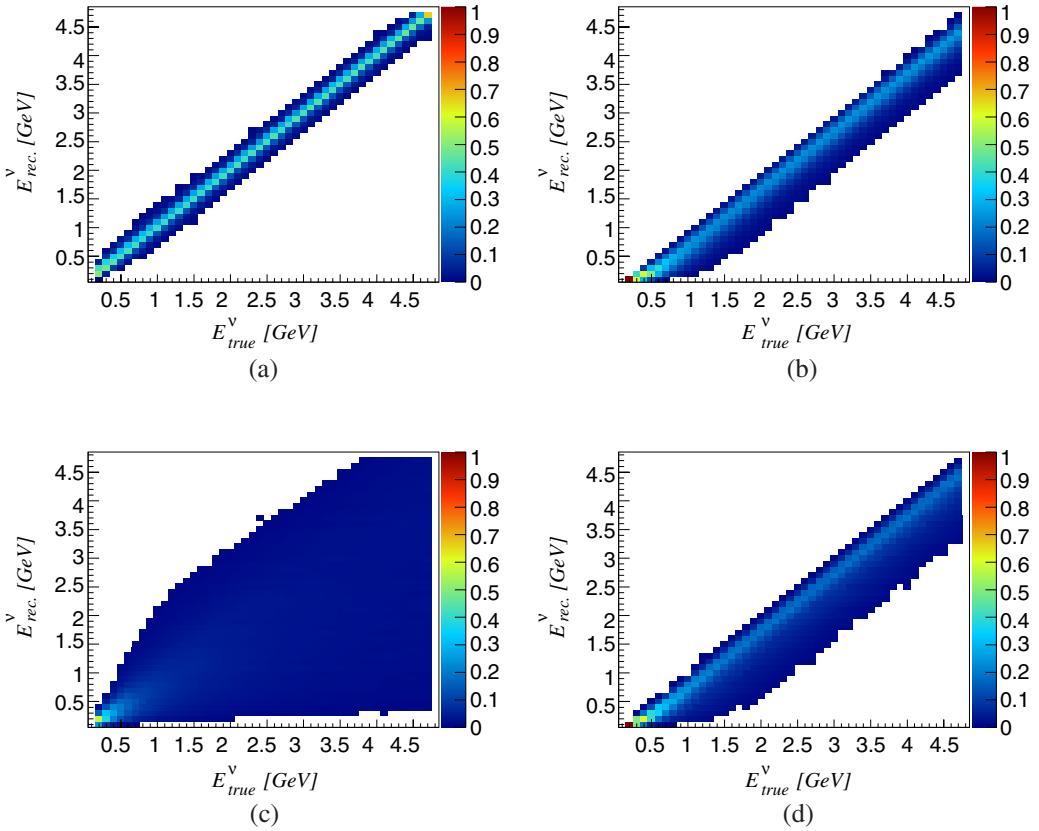


FIG. 8 (color online). Two-dimensional migration matrices ($M_{ij}$), for QE (a), RES (b), MEC/2p2h (c), and non-RES (d) for GiBUU, using $^{16}$O as the target nucleus.

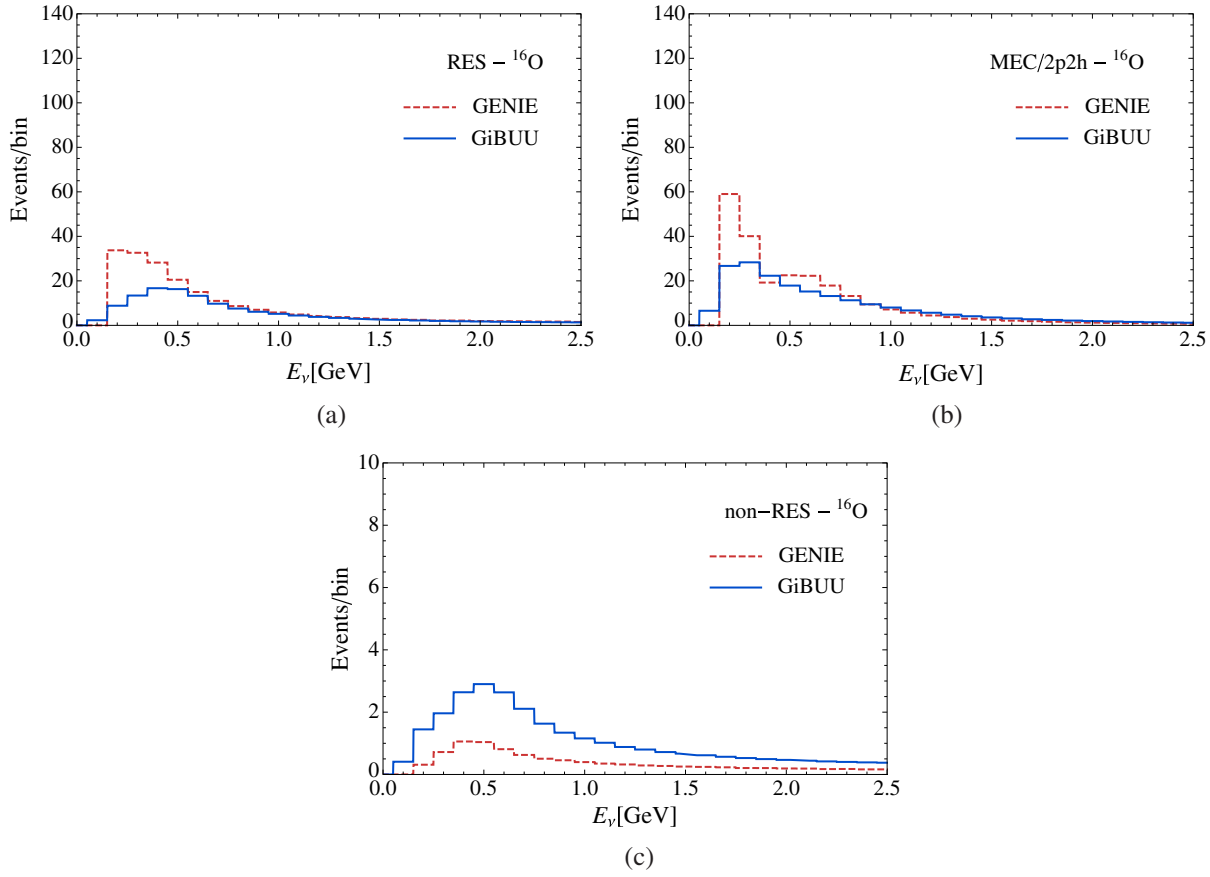


FIG. 9 (color online). Event distributions as a function of the reconstructed neutrino energy for both GENIE (dashed red lines) and GiBUU (solid blue lines), for the non-QE contributions to the QE-like sample. In both cases, oxygen is used as the target nucleus to obtain the cross sections and migration matrices. The different panels show the event distributions for RES (a), MEC/2p2h (b), and non-RES (c) events. The oscillation parameters have been set to their values in Eq. (A1), and detection efficiencies have already been accounted for.


[1] K. Abe *et al.* (T2K Collaboration), Phys. Rev. Lett. **107**, 041801 (2011).
[2] Y. Abe *et al.* (DOUBLE-CHOOZ Collaboration), Phys. Rev. Lett. **108**, 131801 (2012).
[3] F. An *et al.* (DAYA-BAY Collaboration), Phys. Rev. Lett. **108**, 171803 (2012).
[4] J. Ahn *et al.* (RENO collaboration), Phys. Rev. Lett. **108**, 191802 (2012).
[5] Y. Itow, Nucl. Phys. B, Proc. Suppl. **112**, 3 (2002).
[6] D. Harris *et al.* (MINERvA Collaboration), Reports No. FERMILAB-PUB-04-252, No. JLAB-PHYS-04-52, 2004.
[7] P. Huber, M. Mezzetto, and T. Schwetz, J. High Energy Phys. 03 (2008) 021.
[8] E. Fernandez-Martinez and D. Meloni, Phys. Lett. B **697**, 477 (2011).
[9] D. Meloni and M. Martini, Phys. Lett. B **716**, 186 (2012).
[10] P. Coloma, P. Huber, J. Kopp, and W. Winter, Phys. Rev. D **87**, 033004 (2013).
[11] M. Martini, M. Ericson, and G. Chanfray, Phys. Rev. D **85**, 093012 (2012).
[12] J. Nieves, F. Sanchez, I. Ruiz Simo, and M. Vicente Vacas, Phys. Rev. D **85**, 113008 (2012).
[13] O. Lalakulich, U. Mosel, and K. Gallmeister, Phys. Rev. C **86**, 054606 (2012).
[14] M. Martini, M. Ericson, and G. Chanfray, Phys. Rev. D **87**, 013009 (2013).
[15] U. Mosel, O. Lalakulich, and K. Gallmeister, arXiv:1311.7288 [nucl-th].
[16] P. Coloma and P. Huber, Phys. Rev. Lett. **111**, 221802 (2013).
[17] C. Andreopoulos, A. Bell, D. Bhattacharya, F. Cavanna, J. Dobson *et al.*, Nucl. Instrum. Methods Phys. Res., Sect. A **614**, 87 (2010).

[18] T. Leitner, O. Buss, and U. Mosel, Acta Phys. Pol. B **40**, 2585 (2009).
[19] O. Buss, T. Gaitanos, K. Gallmeister, H. van Hees, M. Kaskulov, O. Lalakulich, A. B. Larionov, T. Leitner, J. Weil, and U. Mosel, Phys. Rep. **512**, 1 (2012).
[20] J. Delorme and M. Ericson, Phys. Lett. B **156**, 263 (1985).
[21] J. Marteau, J. Delorme, and M. Ericson, Nucl. Instrum. Methods Phys. Res., Sect. A **451**, 76 (2000).
[22] M. Martini, M. Ericson, G. Chanfray, and J. Marteau, Phys. Rev. C **80**, 065501 (2009).
[23] E. Moniz, I. Sick, R. Whitney, J. Ficenec, R. Kephart, and W. Trower, Phys. Rev. Lett. **26**, 445 (1971).
[24] J. Van Orden and T. Donnelly, Ann. Phys. (N.Y.) **131**, 451 (1981).
[25] T. Leitner and U. Mosel, Phys. Rev. C **81**, 064614 (2010).
[26] D. Drakoulakos *et al.* (Minerva Collaboration), Report No. FERMILAB-PROPOSAL-0938, 2004.
[27] P. Adamson *et al.* (MINOS Collaboration), Phys. Rev. D **77**, 072002 (2008).
[28] H. Chen *et al.* (MicroBooNE Collaboration), Report No. FERMILAB-PROPOSAL-0974, 2007.
[29] D. Ayres *et al.* (NOvA Collaboration), Report No. FERMILAB-PROPOSAL-0929, 2004.
[30] LBNE Conceptual Design Report from October 2012, volume 1, https://sharepoint.fnal.gov/project/lbne/LBNE%20at%20Work/SitePages/Reports%20and%20Documents.aspx.
[31] C. Adams *et al.* (LBNE Collaboration), arXiv:1307.7335.
[32] Y. Hayato, Acta Phys. Pol. B **40**, 2477 (2009).
[33] R. Smith and E. Moniz, Nucl. Phys. **B43**, 605 (1972).
[34] O. Benhar, D. Day, and I. Sick, Rev. Mod. Phys. **80**, 189 (2008).
[35] O. Benhar, N. Farina, H. Nakamura, M. Sakuda, and R. Seki, Phys. Rev. D **72**, 053005 (2005).
[36] O. Benhar and D. Meloni, Nucl. Phys. **A789**, 379 (2007).
[37] A. Bodek and J. Ritchie, Phys. Rev. D **24**, 1400 (1981).
[38] T. Leitner, O. Buss, L. Alvarez-Ruso, and U. Mosel, Phys. Rev. C **79**, 034601 (2009).
[39] R. Bradford, A. Bodek, H. S. Budd, and J. Arrington, Nucl. Phys. B, Proc. Suppl. **159**, 127 (2006).
[40] A. Bodek, S. Avvakumov, R. Bradford, and H. S. Budd, Eur. Phys. J. C **53**, 349 (2008).
[41] T. Leitner, L. Alvarez-Ruso, and U. Mosel, Phys. Rev. C **73**, 065502 (2006).
[42] D. Drechsel and L. Tiator, J. Phys. G **18**, 449 (1992).
[43] D. Drechsel, O. Hanstein, S. Kamalov, and L. Tiator, Nucl. Phys. **A645**, 145 (1999).
[44] L. Alvarez-Ruso, S. Singh, and M. Vicente Vacas, Phys. Rev. C **59**, 3386 (1999).
[45] D. Rein and L. Sehgal, Phys. Lett. B **104**, 394 (1981).
[46] S. Dytman, Acta Phys. Pol. B **40**, 2445 (2009).
[47] M. Martini, M. Ericson, G. Chanfray, and J. Marteau, Phys. Rev. C **81**, 045502 (2010).
[48] O. Benhar, P. Coletti, and D. Meloni, Phys. Rev. Lett. **105**, 132301 (2010).
[49] J. Amaro, M. Barbaro, J. Caballero, T. Donnelly, and C. Williamson, Phys. Lett. B **696**, 151 (2011).
[50] C. Juszczak, J. T. Sobczyk, and J. Zmuda, Phys. Rev. C **82**, 045502 (2010).
[51] A. Bodek, H. Budd, and M. Christy, Eur. Phys. J. C **71**, 1726 (2011).
[52] J. Nieves, I. Ruiz Simo, and M. Vicente Vacas, Phys. Rev. C **83**, 045501 (2011).
[53] J. Nieves, I. Ruiz Simo, and M. Vicente Vacas, Phys. Lett. B **707**, 72 (2012).
[54] M. Martini, M. Ericson, and G. Chanfray, Phys. Rev. C **84**, 055502 (2011).
[55] O. Lalakulich, K. Gallmeister, and U. Mosel, Phys. Rev. C **86**, 014614 (2012).
[56] O. Benhar, A. Lovato, and N. Rocco, arXiv:1312.1210.
[57] O. Benhar and N. Rocco, arXiv:1310.3869.
[58] R. Gran, J. Nieves, F. Sanchez, and M. Vicente Vacas, Phys. Rev. D **88**, 113007 (2013).
[59] A. Aguilar-Arevalo *et al.* (MiniBooNE Collaboration), Phys. Rev. D **81**, 092005 (2010).
[60] T. Katori, arXiv:1304.6014.
[61] S. Boyd, S. Dytman, E. Hernandez, J. Sobczyk, and R. Tacik, AIP Conf. Proc. **1189**, 60 (2009).
[62] S. Nakamura, T. Sato, T. -S. Lee, B. Szczerbinska, and K. Kubodera, Phys. Rev. C **81**, 035502 (2010).
[63] S. X. Nakamura, J. Phys. Conf. Ser. **408**, 012043 (2013).
[64] D. Rein and L. M. Sehgal, Nucl. Phys. **B223**, 29 (1983).
[65] T. Leitner, U. Mosel, and S. Winkelmann, Phys. Rev. C **79**, 057601 (2009).
[66] P. Huber, M. Lindner, T. Schwetz, and W. Winter, J. High Energy Phys. 11 (2009) 044.
[67] V. Bernard, L. Elouadrhiri, and U. Meissner, J. Phys. G **28**, R1 (2002).
[68] M. Gonzalez-Garcia, M. Maltoni, J. Salvado, and T. Schwetz, J. High Energy Phys. 12 (2012) 123.
[69] G. Fiorentini *et al.* (MINERvA Collaboration), Phys. Rev. Lett. **111**, 022502 (2013).
[70] J. Nieves, I. Ruiz Simo, and M. Vicente Vacas, Phys. Lett. B **721**, 90 (2013).
[71] A. Aguilar-Arevalo *et al.* (MiniBooNE Collaboration), Phys. Rev. D **88**, 032001 (2013).
[72] L. Fields *et al.* (MINERvA Collaboration), Phys. Rev. Lett. **111**, 022501 (2013).
[73] K. Abe, T. Abe, H. Aihara, Y. Fukuda, Y. Hayato *et al.*, arXiv:1109.3262.
[74] E. Baussan *et al.* (ESSnuSB Collaboration), arXiv:1309.7022.
[75] A. Stahl, C. Wiebusch, A. Guler, M. Kamiscioglu, R. Sever *et al.*, Reports No. CERN-SPSC-2012-021 and No. SPSC-EOI-007, 2012.
[76] J. Amaro, M. Barbaro, J. Caballero, and T. Donnelly, Phys. Rev. Lett. **108**, 152501 (2012).
[77] M. Martini and M. Ericson, Phys. Rev. C **87**, 065501 (2013).
[78] K. Abe *et al.* (T2K Collaboration), Phys. Rev. D **88**, 032002 (2013).
[79] P. Huber, M. Lindner, and W. Winter, Comput. Phys. Commun. **167**, 195 (2005).
[80] P. Huber, J. Kopp, M. Lindner, M. Rolinec, and W. Winter, Comput. Phys. Commun. **177**, 432 (2007).